

GAMMA-RAY BLAZARS WITHIN THE FIRST 2 BILLION YEARS

M. ACKERMANN², M. AJELLO^{3,1}, L. BALDINI⁴, J. BALLE⁵, G. BARBIELLINI^{6,7}, D. BASTIERI^{8,9}, J. BECERRA GONZALEZ^{10,11},
R. BELLAZZINI¹², E. BISSALDI¹³, R. D. BLANDFORD¹⁴, E. D. BLOOM¹⁴, R. BONINO^{15,16}, E. BOTTACINI¹⁴, J. BREGEON¹⁷,
P. BRUEL¹⁸, R. BUEHLER², S. BUSON^{10,19}, R. A. CAMERON¹⁴, M. CARAGIULO^{20,13}, P. A. CARAVEO²¹, E. CAVAZZUTI²²,
C. CECCHI^{23,24}, C. C. CHEUNG²⁵, J. CHIANG¹⁴, G. CHIARO⁹, S. CIPRINI^{22,23}, J. CONRAD^{26,27,28}, D. COSTANTIN⁹, F. COSTANZA¹³,
S. CUTINI^{22,23}, F. D'AMMANDO^{29,30}, F. DE PALMA^{13,31}, R. DESIANTE^{15,32}, S. W. DIGEL¹⁴, N. DI LALLA⁴, M. DI MAURO¹⁴,
L. DI VENERE^{20,13}, A. DOMÍNGUEZ³, P. S. DRELL¹⁴, C. FAVUZZI^{20,13}, S. J. FEGAN¹⁸, E. C. FERRARA¹⁰, J. FINKE²⁵, W. B. FOCKE¹⁴,
Y. FUKAZAWA³³, S. FUNK³⁴, P. FUSCO^{20,13}, F. GARGANO¹³, D. GASPARRINI^{22,23,1}, N. GIGLIETTO^{20,13}, F. GIORDANO^{20,13},
M. GIROLETTI²⁹, D. GREEN^{11,10}, I. A. GRENIER⁵, L. GUILLEMOT^{35,36}, S. GUIRIEC^{10,19}, D. H. HARTMANN³, E. HAYS¹⁰, D. HORAN¹⁸,
T. JOGLER³⁷, G. JÓHANNESSEN³⁸, A. S. JOHNSON¹⁴, M. KUSS¹², G. LA MURA⁹, S. LARSSON^{39,27}, L. LATRONICO¹⁵, J. LI⁴⁰,
F. LONGO^{6,7}, F. LOPARCO^{20,13}, M. N. LOVELLETTE²⁵, P. LUBRANO²³, J. D. MAGILL¹¹, S. MALDERA¹⁵, A. MANFREDA⁴,
L. MARCOTULLI³, M. N. MAZZIOTTA¹³, P. F. MICHELSON¹⁴, N. MIRABAL^{10,19}, W. MITTHUMSIRI⁴¹, T. MIZUNO⁴², M. E. MONZANI¹⁴,
A. MORSELLI⁴³, I. V. MOSKALENKO¹⁴, M. NEGRO^{15,16}, E. NUSS¹⁷, T. OHSUGI⁴², R. OJHA^{10,1}, N. OMODEI¹⁴, M. ORIENTI²⁹,
E. ORLANDO¹⁴, J. F. ORMES⁴⁴, V. S. PALIYA^{3,1}, D. PANEQUE⁴⁵, J. S. PERKINS¹⁰, M. PERSIC^{6,46}, M. PESCE-ROLLINS¹², F. PIRON¹⁷,
T. A. PORTER¹⁴, G. PRINCIPE³⁴, S. RAINÒ^{20,13}, R. RANDO^{8,9}, B. RANI¹⁰, M. RAZZANO^{12,47}, S. RAZZAQUE⁴⁸, A. REIMER^{49,14},
O. REIMER^{49,14}, R. W. ROMANI¹⁴, C. SGRO¹², D. SIMONE¹³, E. J. SISKIND⁵⁰, F. SPADA¹², G. SPANDRE¹², P. SPINELLI^{20,13},
C. S. STALIN⁵¹, L. STAWARZ⁵², D. J. SUSON⁵³, M. TAKAHASHI⁴⁵, K. TANAKA³³, J. B. THAYER¹⁴, D. J. THOMPSON¹⁰,
D. F. TORRES^{40,54}, E. TORRESI⁵⁵, G. TOSTI^{23,24}, E. TROJA^{10,11}, G. VIANELLO¹⁴, K. S. WOOD⁵⁶

¹Corresponding authors: M. Ajello, majello@g.clemson.edu; D. Gasparrini, gasparrini@asdc.asi.it; R. Ojha, roopesh.ojha@gmail.com; V. S. Paliya, vpaliya@g.clemson.edu.

²Deutsches Elektronen Synchrotron DESY, D-15738 Zeuthen, Germany

³Department of Physics and Astronomy, Clemson University, Kinard Lab of Physics, Clemson, SC 29634-0978, USA

⁴Università di Pisa and Istituto Nazionale di Fisica Nucleare, Sezione di Pisa I-56127 Pisa, Italy

⁵Laboratoire AIM, CEA-IRFU/CNRS/Université Paris Diderot, Service d'Astrophysique, CEA Saclay, F-91191 Gif sur Yvette, France

⁶Istituto Nazionale di Fisica Nucleare, Sezione di Trieste, I-34127 Trieste, Italy

⁷Dipartimento di Fisica, Università di Trieste, I-34127 Trieste, Italy

⁸Istituto Nazionale di Fisica Nucleare, Sezione di Padova, I-35131 Padova, Italy

⁹Dipartimento di Fisica e Astronomia "G. Galilei", Università di Padova, I-35131 Padova, Italy

¹⁰NASA Goddard Space Flight Center, Greenbelt, MD 20771, USA

¹¹Department of Physics and Department of Astronomy, University of Maryland, College Park, MD 20742, USA

¹²Istituto Nazionale di Fisica Nucleare, Sezione di Pisa, I-56127 Pisa, Italy

¹³Istituto Nazionale di Fisica Nucleare, Sezione di Bari, I-70126 Bari, Italy

¹⁴W. W. Hansen Experimental Physics Laboratory, Kavli Institute for Particle Astrophysics and Cosmology, Department of Physics and SLAC National Accelerator Laboratory, Stanford University, Stanford, CA 94305, USA

¹⁵Istituto Nazionale di Fisica Nucleare, Sezione di Torino, I-10125 Torino, Italy

¹⁶Dipartimento di Fisica, Università degli Studi di Torino, I-10125 Torino, Italy

¹⁷Laboratoire Univers et Particules de Montpellier, Université Montpellier, CNRS/IN2P3, F-34095 Montpellier, France

¹⁸Laboratoire Leprince-Ringuet, École polytechnique, CNRS/IN2P3, F-91128 Palaiseau, France

¹⁹NASA Postdoctoral Program Fellow, USA

²⁰Dipartimento di Fisica "M. Merlin" dell'Università e del Politecnico di Bari, I-70126 Bari, Italy

²¹INAF-Istituto di Astrofisica Spaziale e Fisica Cosmica Milano, via E. Bassini 15, I-20133 Milano, Italy

²²Agenzia Spaziale Italiana (ASI) Science Data Center, I-00133 Roma, Italy

²³Istituto Nazionale di Fisica Nucleare, Sezione di Perugia, I-06123 Perugia, Italy

²⁴Dipartimento di Fisica, Università degli Studi di Perugia, I-06123 Perugia, Italy

²⁵Space Science Division, Naval Research Laboratory, Washington, DC 20375-5352, USA

²⁶Department of Physics, Stockholm University, AlbaNova, SE-106 91 Stockholm, Sweden

²⁷The Oskar Klein Centre for Cosmoparticle Physics, AlbaNova, SE-106 91 Stockholm, Sweden

²⁸Wallenberg Academy Fellow

²⁹INAF Istituto di Radioastronomia, I-40129 Bologna, Italy

³⁰Dipartimento di Astronomia, Università di Bologna, I-40127 Bologna, Italy

³¹Università Telematica Pegaso, Piazza Trieste e Trento, 48, I-80132 Napoli, Italy

- ³²Università di Udine, I-33100 Udine, Italy
- ³³Department of Physical Sciences, Hiroshima University, Higashi-Hiroshima, Hiroshima 739-8526, Japan
- ³⁴Erlangen Centre for Astroparticle Physics, D-91058 Erlangen, Germany
- ³⁵Laboratoire de Physique et Chimie de l'Environnement et de l'Espace – Université d'Orléans / CNRS, F-45071 Orléans Cedex 02, France
- ³⁶Station de radioastronomie de Nançay, Observatoire de Paris, CNRS/INSU, F-18330 Nançay, France
- ³⁷Friedrich-Alexander-Universität, Erlangen-Nürnberg, Schlossplatz 4, 91054 Erlangen, Germany
- ³⁸Science Institute, University of Iceland, IS-107 Reykjavik, Iceland
- ³⁹Department of Physics, KTH Royal Institute of Technology, AlbaNova, SE-106 91 Stockholm, Sweden
- ⁴⁰Institute of Space Sciences (IEEC-CSIC), Campus UAB, Carrer de Magrans s/n, E-08193 Barcelona, Spain
- ⁴¹Department of Physics, Faculty of Science, Mahidol University, Bangkok 10400, Thailand
- ⁴²Hiroshima Astrophysical Science Center, Hiroshima University, Higashi-Hiroshima, Hiroshima 739-8526, Japan
- ⁴³Istituto Nazionale di Fisica Nucleare, Sezione di Roma "Tor Vergata", I-00133 Roma, Italy
- ⁴⁴Department of Physics and Astronomy, University of Denver, Denver, CO 80208, USA
- ⁴⁵Max-Planck-Institut für Physik, D-80805 München, Germany
- ⁴⁶Osservatorio Astronomico di Trieste, Istituto Nazionale di Astrofisica, I-34143 Trieste, Italy
- ⁴⁷Funded by contract FIRB-2012-RBFR12PM1F from the Italian Ministry of Education, University and Research (MIUR)
- ⁴⁸Department of Physics, University of Johannesburg, PO Box 524, Auckland Park 2006, South Africa
- ⁴⁹Institut für Astro- und Teilchenphysik und Institut für Theoretische Physik, Leopold-Franzens-Universität Innsbruck, A-6020 Innsbruck, Austria
- ⁵⁰NYCB Real-Time Computing Inc., Lattingtown, NY 11560-1025, USA
- ⁵¹Indian Institute of Astrophysics, Block II, Koramangala, Bangalore 560034, India
- ⁵²Astronomical Observatory, Jagiellonian University, 30-244 Kraków, Poland
- ⁵³Department of Chemistry and Physics, Purdue University Calumet, Hammond, IN 46323-2094, USA
- ⁵⁴Institució Catalana de Recerca i Estudis Avançats (ICREA), E-08010 Barcelona, Spain
- ⁵⁵INAF-Istituto di Astrofisica Spaziale e Fisica Cosmica Bologna, via P. Gobetti 101, I-40129 Bologna, Italy
- ⁵⁶Praxis Inc., Alexandria, VA 22303, resident at Naval Research Laboratory, Washington, DC 20375, USA

ABSTRACT

The detection of high-redshift ($z > 3$) blazars enables the study of the evolution of the most luminous relativistic jets over cosmic time. More importantly, high-redshift blazars tend to host massive black holes and can be used to constrain the space density of heavy black holes in the early Universe. Here, we report the first detection with the *Fermi*-Large Area Telescope of five γ -ray emitting blazars beyond $z = 3.1$, more distant than any blazars previously detected in γ -rays. Among these five objects, NVSS J151002+570243 is now the most distant known γ -ray emitting blazar at $z = 4.31$. These objects have steeply falling γ -ray spectral energy distributions (SEDs) and, those that have been observed in X-rays, a very hard X-ray spectrum, both typical of powerful blazars. Their Compton dominance (ratio of the inverse Compton to synchrotron peak luminosities) is also very large (> 20). All of these properties place these objects among the most extreme members of the blazar population. Their optical spectra and the modeling of their optical-UV SEDs confirm that these objects harbor massive black holes ($M_{\text{BH}} \sim 10^8\text{--}10^{10}M_{\odot}$). We find that, at $z \approx 4$, the space density of $> 10^9M_{\odot}$ black holes hosted in radio-loud and radio-quiet active galactic nuclei are similar, implying that radio-loudness may play a key role in rapid black hole growth in the early Universe.

Keywords: galaxies: active — gamma rays: galaxies— galaxies: jets— galaxies: high-redshift— quasars: general

1. INTRODUCTION

Blazars are the most powerful Active Galactic Nuclei (AGN) with relativistic jets oriented close to the line of sight. The jet radiation dominates their broadband emission, especially at γ -rays where the inverse Compton (IC) hump of the blazar spectral energy distribution (SED) peaks around tens or hundreds of MeV. The Large Area Telescope (LAT) onboard the *Fermi* satellite (Atwood et al. 2009) has

already detected thousands of blazars, thus confirming that they are the most numerous population in the γ -ray sky (e.g., Ackermann et al. 2015). Nonetheless, high-redshift blazars above a redshift of 3.1 are missing in the *Fermi* catalogs, possibly due to the shift of the IC peak to lower frequencies in which LAT is less sensitive. The newly released Pass 8 photon data set (Atwood et al. 2013), with an improved event-level analysis, substantially enhances the sensitivity of the LAT at all energies and in particular at lower energies (i.e.,

<200 MeV). This increases the capability of the LAT to detect spectrally soft, potentially high- z blazars.

These objects typically have large bolometric luminosities ($L_{\text{bol.}} > 10^{48}$ erg s $^{-1}$) and host powerful relativistic jets ($P_j \gtrsim \dot{M}c^2$ for a given accretion efficiency; e.g., Ghisellini et al. 2014). In general, they harbor extremely massive black holes ($M_{\text{BH}} \sim 10^9 M_{\odot}$; Ghisellini et al. 2010). Since blazars are highly beamed, the detection of a single blazar implies the existence of $2\Gamma^2$ (i.e., ~ 400 – 600 , Γ is the bulk Lorentz factor) misaligned blazars with similar properties. Therefore, the detection of high- z blazars can constrain models of supermassive black hole formation in the early Universe (see, e.g., Volonteri et al. 2011; Ghisellini et al. 2013). This suggests that the detection of new high- z blazars will test the hypotheses of blazar evolution, since these high redshifts constrain the time available for such extreme objects to grow.

Motivated by the recent release of the sensitive Pass 8 dataset, we perform a systematic search for new γ -ray emitters beyond $z = 3.1$ and in this Letter we report the first detection of five $z > 3.1$ γ -ray emitting blazars. Throughout, we adopt a Λ CDM cosmology with the Hubble constant $H_0 = 71$ km s $^{-1}$ Mpc $^{-1}$, $\Omega_m = 0.27$, and $\Omega_{\Lambda} = 0.73$.

2. SAMPLE SELECTION AND ANALYSIS

In order to search for high- z blazars, we start from the ~ 1.4 million quasars included in the Million Quasar Catalog (MQC; Flesch 2015). We select all $z > 3.1$ sources and retain only radio-loud (RL) quasars with $R > 10$, where R is the ratio of the rest-frame 5 GHz (extrapolated from 1.4 GHz, considering a flat radio spectrum) to optical B band flux density (Kellermann et al. 1989), assuming an optical spectral index -0.5 ($F_{\nu} \propto \nu^{\alpha}$). These 1103 objects¹ represent our parent sample and we analyze LAT data for all of them according to the following procedure.

For each object we use ~ 92 months (from 2008 August 5 to 2016 April 1) of *Fermi* Pass 8 source class photons and analyze them following the standard data reduction procedure², but with a few modifications as mentioned below. We define a region of interest (ROI) of 15° radius centered on each quasar and define a sky model that includes all γ -ray sources detected in the third *Fermi*-LAT catalog (3FGL; Acero et al. 2015), within the ROI and the isotropic and Galactic diffuse emission models (Acero et al. 2016). The parameters of all sources within the ROI and power-law normalization factors of the diffuse models are optimized so that the sky model reproduces the data as best as possible. This is done via a binned likelihood method and we measure the significance of the detection by means of the maximum likelihood test statistic $\text{TS} = 2\Delta \log \mathcal{L}$, where \mathcal{L} represents the likelihood function,

between models with and without a point source at the position of the quasar. The targets of interest are modeled with a simple power-law model leaving the prefactor and the photon index free to vary during the likelihood fitting. We consider a source to be significantly detected if $\text{TS} > 25$ (4.2σ ; Mattox et al. 1996).

Since we are dealing with faint sources, we modify the standard data reduction procedure as follows. We expand the energy range considered so it spans 60 MeV to 300 GeV. This allows the analysis to be more sensitive to spectrally soft γ -ray sources, i.e., blazars whose high-energy peak is shifted to lower energies (~ 1 – 10 MeV) as typical for high- z blazars. Moreover, Pass 8 provides an increase in the acceptance at < 100 MeV by up to 75%, with respect to Pass 7, which translates into an improved sensitivity for high- z blazars. Because the energy resolution becomes increasingly worse at low energies we enable the energy dispersion correction in the analysis for all sources except the empirical diffuse models. A novelty introduced by Pass 8 is the characterization of the photons in PSF (point-spread function) type events, which sub-classify the events into four quartiles by quality of angular reconstruction, with the lowest quartile (PSF0) and highest quartile (PSF3) having the worst and the best, respectively, direction reconstruction. In order to take full advantage of this improvement, we perform a component-wise data analysis for each PSF event type by considering the product of the likelihood function (sum of the logarithms) for the four PSF event types, using the SUMMED likelihood method of the Science Tools³.

As in the case of our target sources, there could be faint gamma-ray emitters present in the data but not in the 3FGL catalog. Thus, we rely on an iterative procedure to discover, localize, and insert such sources into the sky model. This is done by generating a residual TS map for each ROI. The spatial positions of unmodeled excesses with $\text{TS} \geq 25$ are optimized and inserted into the sky model with power-law spectra. This procedure is iterated until no significant unmodeled emission remains in the ROI.

3. RESULTS AND DISCUSSION

Our systematic search for significant γ -ray emitters among a large sample of RL quasars has led to the detection of five sources. A likelihood ratio (LR) method (see Ackermann et al. 2011, for details) associates the detected γ -ray sources and their radio counterparts (from NRAO VLA Sky Survey or NVSS; Condon et al. 1998) with high confidence (association probability $> 80\%$). By repeating the LAT analysis adopting 1000 random positions drawn from a randomized NVSS catalog⁴, we found that the probability that

¹ We exclude all the objects with a photometric redshift in MQC.

² <http://fermi.gsfc.nasa.gov/ssc/data/analysis/documentation/>

³ <http://fermi.gsfc.nasa.gov/ssc/data/analysis/software/>

⁴ The NVSS catalog is randomized by mirroring the Galactic longitudes (glon) of the sources to $360^{\circ} - \text{glon}$.

any of the newly detected γ -ray sources are spurious is negligible. The basic information for these objects is presented in Table 1 where we also show the results of the LAT data analysis. As can be seen, all the objects are extremely RL and γ -ray luminous quasars. According to our analysis, NVSS J151002+570243 ($z = 4.31$) is now the farthest known γ -ray emitting blazar⁵. In Figure 1, we show residual TS maps of five detected objects, along with their radio and optimized γ -ray positions.

In general, high-redshift blazars are brighter at hard X-rays than in the γ -ray band (e.g., Romani 2006; Sbarrato et al. 2013), probably due to the shift of the blazar SED to lower frequencies. This could be due to the intrinsic shift of the high-energy peak to lower energies as the bolometric non-thermal luminosity increases (Fossati et al. 1998; Donato et al. 2001). Another possible reason for the shift could be the fact that the high-energy emission of such high-redshift blazars is powered via IC scattering off photons from the torus rather than the broad-line region (BLR), which also contributes to the lowering of the frequency of their SED peak (Sikora et al. 2002). Alternatively, the SED peaks can also shift to lower energies provided the emission region is within the dense BLR photon field. In this case, an efficient cooling of the emitting electrons will cause the lowering of the SED peaks (Ghisellini et al. 1998). The shift of the SED causes their γ -ray spectra to become steeper and to move slightly outside, or at the limit, of the *Fermi*-LAT band. Indeed, all the blazars discovered here exhibit steep γ -ray spectra ($\Gamma_\gamma > 2.5$, see Table 1). This suggests their IC peak lie at MeV energies.

In Figure 2, we compare these newly detected distant objects with the blazars included in the third catalog of *Fermi*-LAT detected AGN (3LAC; Ackermann et al. 2015). As can be seen in the left panel, these sources occupy the region of high γ -ray luminosities ($L_\gamma > 10^{47}$ erg s⁻¹) and soft photon indices ($\Gamma_\gamma > 2.5$), typical of powerful blazars. The right panel of Figure 2 compares the redshift distributions of these newly discovered high- z blazars with that of the 3LAC blazars. Though the population of distant blazars is small, this work opens a window for the study of high- z blazars and may have a major impact on constraining the various physical parameters associated with the blazar population (see, e.g., Paliya et al. 2016, for a relevant discussion).

In order to understand the broadband behavior of these high- z blazars we look into the literature for multi-frequency information. Though there is a paucity of such data, we found a few noteworthy observations that support the blazar nature of these objects. NVSS J064632+445116 was predicted as a candidate γ -ray emitter by Healey et al.

(2008), whereas NVSS J135406–020603 is included in the ROMA-BZCAT (Massaro et al. 2015). The quasar NVSS J212912–153841 is a hard X-ray spectrum luminous blazar and included in the 70 month *Swift*-Burst Alert Telescope catalog (Baumgartner et al. 2013). NVSS J151002+570243 is one of the best studied among all of the objects and exhibits an intense and hard X-ray spectrum (e.g., Mathur & Elvis 1995; Moran & Helfand 1997; Wu et al. 2013).

We generate broadband SEDs of the three objects that have archival X-ray observations and model them using a simple one zone synchrotron-IC emission approach prescribed in Ghisellini & Tavecchio (2009). In brief, the model assumes a spherical emission region located at a distance R_{diss} from the central engine and filled with a population of highly energetic electrons that follow a broken power-law distribution. In the presence of a tangled magnetic field, the electrons lose energy via synchrotron, synchrotron self Compton (SSC), and external Compton (EC) processes. For the latter, the seed photons originate from several external AGN components: photons directly emitted from the accretion disk (e.g., Dermer & Schlickeiser 1993), from BLR (Sikora et al. 1994) and from the infrared torus (e.g., Błażejowski et al. 2000). The calculated jet powers and SED parameters are given in Table 2 and the modeled SEDs are shown in Figure 3.

In each of the three objects, the IR-UV emission is found to be dominated by an extremely luminous accretion disk ($L_{\text{disk}} > 10^{46}$ erg s⁻¹). The X-ray spectra, on the other hand, are hard and the entire X-ray to γ -ray band of the SED can be explained by the IC scattering off the photons originating from the BLR. A strong accretion disk radiation implies a dense BLR photon field surrounding the jet, which in turn is observable in the form of broad optical emission lines. According to our SED modeling analysis, a large BLR radiative energy density indicates that most of the high-energy emission originates from the interaction of the BLR photons with the jet electrons. This suggests that the cooling of the electrons will be efficient, and accordingly the synchrotron emission will peak at low frequencies, which is supported by the modeling results. This indicates the location of the γ -ray emitting region to be inside the BLR. However, it should be noted that with the sparse available observations, it is not possible to tightly constrain the location of the emission region. The Compton dominance (ratio of the IC to synchrotron peak luminosities) of each of the three sources is also very large (> 20 , Table 2), a characteristic feature exhibited by powerful blazars. Other SED parameters are similar to those generally observed in high- z blazars (e.g., Ghisellini et al. 2010). Though the data used here are mostly non-simultaneous, they indicate a *typical* state of the blazar rather than any period of specific activity. Also, the γ -ray photon statistics are not good enough to search for temporal variability. Overall, the *Fermi*-LAT detection and the available data confirm the blazar nature of the 5 high- z RL quasars.

Powerful blazars are generally found to host massive black

⁵ The blazar QSO J0906+6930 discovered at $z = 5.48$ by Romani et al. (2004) was found to be spatially coincident with a 1.5σ EGRET fluctuation, but it has not been confirmed as a γ -ray source.

holes at their centers (e.g., Ghisellini et al. 2010; Paliya et al. 2016). It is, therefore, of great interest to determine the black hole mass of these γ -ray detected quasars. In Table 1, we report the black hole masses for each of the five sources using information that we could find/derive from the optical spectroscopic information available in the literature (Torrealba et al. 2012; Alam et al. 2015). Furthermore, we also derive the masses by modeling the observed IR-UV emission for three objects (Figure 3) with a standard Shakura & Sunyaev (1973) accretion disk and the results are presented in Table 2. Both methods predict the existence of massive black holes ($\sim 10^{8-10} M_{\odot}$) and match reasonably well within a factor of \sim three⁶, except for NVSS J151002+570243, for which the modeling approach predicts a higher black hole mass. In particular, the object NVSS J212912–153841 hosts one of the most massive black holes, $\sim 7 \times 10^9 M_{\odot}$, ever found in γ -ray emitting blazars, confirmed both from optical spectroscopic and disk modeling approaches.

At redshifts between 3 and 4, the space density of black holes with $M_{\text{BH}} > 10^9 M_{\odot}$ hosted in jetted AGN is 50 Gpc^{-3} (Sbarato et al. 2015). This estimate is based on the luminosity function reported in Ajello et al. (2009), which, at those redshifts, relies only on five blazars. This work finds two more blazars hosting massive black holes ($M_{\text{BH}} > 10^9 M_{\odot}$) in the same redshift range, considering black hole masses derived from the optical spectroscopic information. Adopting $\Gamma = 13$, derived from our SED modeling, these two objects imply the presence of ~ 675 (i.e., $2 \times 2\Gamma^2$) similar systems, but with jets pointing in all directions, in the same redshift bin. The number density related to these two sources can be computed as $n = 675 / (V_{\text{MAX}} \times f_{\text{sky}} \times f_{\text{prob}} \times f_z) \approx 18 \text{ Gpc}^{-3}$, where $f_{\text{sky}}=0.52$ is the fraction of the sky covered by our parent sample, $f_z=0.84$ is the

fraction of sources in the parent sample with a spectroscopic redshift, $f_{\text{prob}}=0.66$ is the fraction of γ -ray sources that are associated and $V_{\text{MAX}} = 134 \text{ Gpc}^{-3}$ is the available volume⁷ where these sources could have been detected (Schmidt 1968). This brings the estimate of the space density of massive black holes hosted in jetted systems to $68_{-24}^{+36} \text{ Gpc}^{-3}$. Already at redshift 4, this implies that there is a similar number of massive black holes hosted in radio-loud and radio-quiet systems and that, given their strong evolution, above that redshift most massive black holes might be hosted in radio-loud systems (Ghisellini et al. 2010; Volonteri et al. 2011). This clearly shows that the radio-loud phase may be a key ingredient for quick black hole growth in the early Universe. To this end, the detection of high- z blazars becomes very important. Currently, the most promising approaches are, (1) lowering the energy threshold of the LAT, and (2) using *NuSTAR*. However, the optimal instrument would be a sensitive all-sky MeV telescope, e.g., e-ASTROGAM (Tatischeff et al. 2016) and AMEGO⁸.

We are grateful to the referee for insightful comments. The *Fermi*-LAT Collaboration acknowledges support for LAT development, operation and data analysis from NASA and DOE (United States), CEA/Irfu and IN2P3/CNRS (France), ASI and INFN (Italy), MEXT, KEK, and JAXA (Japan), and the K.A. Wallenberg Foundation, the Swedish Research Council and the National Space Board (Sweden). Science analysis support in the operations phase from INAF (Italy) and CNES (France) is also gratefully acknowledged. Part of this work is based on archival data, software, or online services provided by the ASI Science Data Center (ASDC).

Facilities: *Fermi*-LAT

REFERENCES

- Acero, F., Ackermann, M., Ajello, M., et al. 2016, *ApJS*, 223, 26
 Acero, F., Ackermann, M., Ajello, M., et al. 2015, *ApJS*, 218, 23
 Ackermann, M., Ajello, M., Allafort, A., et al. 2011, *ApJ*, 743, 171
 Ackermann, M., Ajello, M., Atwood, W. B., et al. 2015, *ApJ*, 810, 14
 Ajello, M., Costamante, L., Sambruna, R. M., et al. 2009, *ApJ*, 699, 603
 Alam, S., Albareti, F. D., Allende Prieto, C., et al. 2015, *ApJS*, 219, 12
 Atwood, W. B., Abdo, A. A., Ackermann, M., et al. 2009, *ApJ*, 697, 1071
 Atwood, W., Albert, A., Baldini, L., et al. 2013, arXiv:1303.3514
 Baumgartner, W. H., Tueller, J., Markwardt, C. B., et al. 2013, *ApJS*, 207, 19
- ⁶ One should keep in mind the large uncertainties (~ 0.4 dex) associated with the virial BH mass estimation methods (see, e.g., Vestergaard & Peterson 2006; Shen et al. 2011).
- ⁷ This has been computed taking into account the detection efficiency of the LAT.
- ⁸ https://pcos.gsfc.nasa.gov/phypag/probe/AMEGO_probe.pdf
- Błażejowski, M., Sikora, M., Moderski, R., & Madejski, G. M. 2000, *ApJ*, 545, 107
 Condon, J. J., Cotton, W. D., Greisen, E. W., et al. 1998, *AJ*, 115, 1693
 Dermer, C. D., & Schlickeiser, R. 1993, *ApJ*, 416, 458
 Donato, D., Ghisellini, G., Tagliaferri, G., & Fossati, G. 2001, *A&A*, 375, 739
 Flesch, E. W. 2015, *PASA*, 32, e010
 Fossati, G., Maraschi, L., Celotti, A., Comastri, A., & Ghisellini, G. 1998, *MNRAS*, 299, 433
 Ghisellini, G., Celotti, A., Fossati, G., Maraschi, L., & Comastri, A. 1998, *MNRAS*, 301, 451
 Ghisellini, G., Haardt, F., Della Ceca, R., Volonteri, M., & Sbarato, T. 2013, *MNRAS*, 432, 2818
 Ghisellini, G., & Tavecchio, F. 2009, *MNRAS*, 397, 985
 Ghisellini, G., Tavecchio, F., Maraschi, L., Celotti, A., & Sbarato, T. 2014, *Nature*, 515, 376
 Ghisellini, G., Della Ceca, R., Volonteri, M., et al. 2010, *MNRAS*, 405, 387
 Healey, S. E., Romani, R. W., Cotter, G., et al. 2008, *ApJS*, 175, 97
 Kellermann, K. I., Sramek, R., Schmidt, M., Shaffer, D. B., & Green, R. 1989, *AJ*, 98, 1195
 Massaro, E., Maselli, A., Leto, C., et al. 2015, *Ap&SS*, 357, 75

Table 1. Basic information and results of the *Fermi*-LAT data analysis of high-redshift blazars.

Basic information							
Name (NVSS)	Radio position (J2000)		$F_{1.4\text{ GHz}}$ (mJy)	R (mag)	z	RL	$M_{\text{BH},s}$ M_{\odot}
	hh mm ss.ss	dd mm ss.s					
J064632+445116	06 46 32.00	+44 51 17.0	452	18.5	3.4	1253	9.1 [§]
J135406–020603	13 54 06.90	–02 06 03.2	733	19.2	3.7	3741	8.9 [†]
J151002+570243	15 10 02.92	+57 02 43.4	202	19.9	4.3	1850	8.5 [†]
J163547+362930	16 35 47.24	+36 29 30.0	152	20.6	3.6	2842	8.7 [†]
J212912–153841	21 29 12.13	–15 38 41.0	590	16.5	3.3	263	9.8 [§]

<i>Fermi</i> -LAT data analysis							
Optimized position (J2000)	$R_{95\%}$ (degrees)	$F_{0.06-300\text{ GeV}}$ ($10^{-8}\text{ ph cm}^{-2}\text{ s}^{-1}$)	Γ_{γ}	L_{γ} ($10^{48}\text{ erg s}^{-1}$)	TS		
						hh mm ss.ss	dd mm ss.s
06 47 22	+45 02 40	0.24	2.03±0.40	2.68±0.10	1.4±0.4	62	
13 54 28	–02 06 43	0.22	2.32±0.52	2.88±0.14	2.5±0.8	44	
15 10 06	+57 05 07	0.18	0.86±0.30	2.55±0.16	1.1±0.5	34	
16 35 44	+36 29 45	0.13	5.31±0.96	3.15±0.14	7.0±0.2	151	
21 28 25	–15 34 25	0.33	2.65±0.43	2.82±0.10	1.9±0.4	66	

NOTE—Name, radio positions, and 1.4 GHz flux values have been adopted from the NVSS catalog. R band magnitude and redshifts are taken from MQC. Radio-loudness (RL) is the ratio of the rest-frame 5 GHz (extrapolated from 1.4 GHz assuming a flat radio spectrum) to optical B band flux density. $M_{\text{BH},s}$ is the logarithmic central black hole mass, in units of solar mass, derived/taken from available optical spectroscopic information: [§]Torrealba et al. (2012), [†]Alam et al. (2015). $R_{95\%}$ is the 95% error radius derived from the analysis. The γ -ray flux and apparent luminosity are in the energy range of 0.06–300 GeV.

Table 2. Summary of the parameters used/derived from the modeling of the SED of the objects shown in Figure 3. The viewing angle is taken as 3° for all of them.

Parameter	J0646+4451	J1510+5702	J2129–1538
Slope of the electron energy distribution before break energy (p)	1.8	1.8	2.2
Slope of the electron energy distribution after break energy (q)	4.4	4.1	4.5
Magnetic field in Gauss (B)	2.1	1.4	1.3
Particle energy density in erg cm^{-3} (U'_e)	0.009	0.029	0.002
Bulk Lorentz factor (Γ)	12	11	14
Minimum Lorentz factor (γ'_{min})	1	1	1
Break Lorentz factor (γ'_b)	72	82	51
Maximum Lorentz factor (γ'_{max})	2e3	3e3	2e3
Size of the emission region in parsec (R_{blob})	0.025	0.017	0.059
Dissipation distance in parsec (R_{diss})	0.25	0.17	0.59
Size of the BLR in parsec (R_{BLR})	0.37	0.22	0.79
Black hole mass in log scale, in units of solar mass ($M_{\text{BH},m}$)	9.60	9.48	9.85
Accretion disk luminosity in log scale (L_{disk} , erg s^{-1})	47.11	46.65	47.78
Accretion disk luminosity in Eddington units ($L_{\text{disk}}/L_{\text{Edd}}$)	0.26	0.12	0.68
Fraction of the disk luminosity reprocessed by the BLR (f_{BLR})	0.1	0.1	0.1
Fraction of the disk luminosity reprocessed by the IR-torus (f_{IR})	0.5	0.5	0.5
Compton dominance (CD)	25	47	99
Jet power in electrons in log scale (P_e , erg s^{-1})	44.88	44.94	45.14
Jet power in magnetic field in log scale (P_B), erg s^{-1})	46.15	45.38	46.58
Radiative jet power in log scale (P_r , erg s^{-1})	45.89	45.70	46.31
Jet power in protons in log scale (P_p , erg s^{-1})	47.38	47.45	47.89

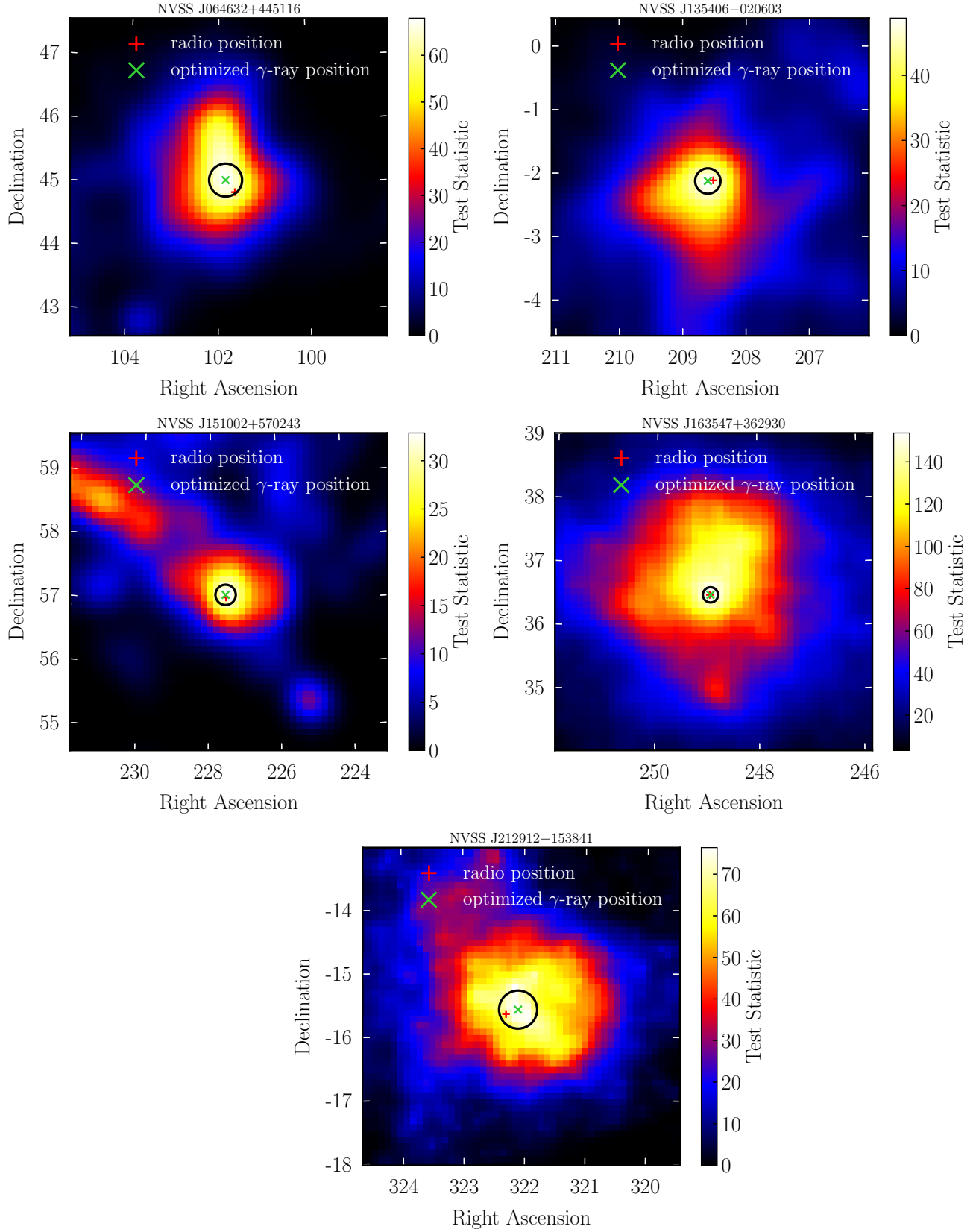


Figure 1. The test statistic maps of five high- z quasars. The radio position (J2000), optimized γ -ray position (J2000) and the associated 95% error circle (in degrees) are also shown.

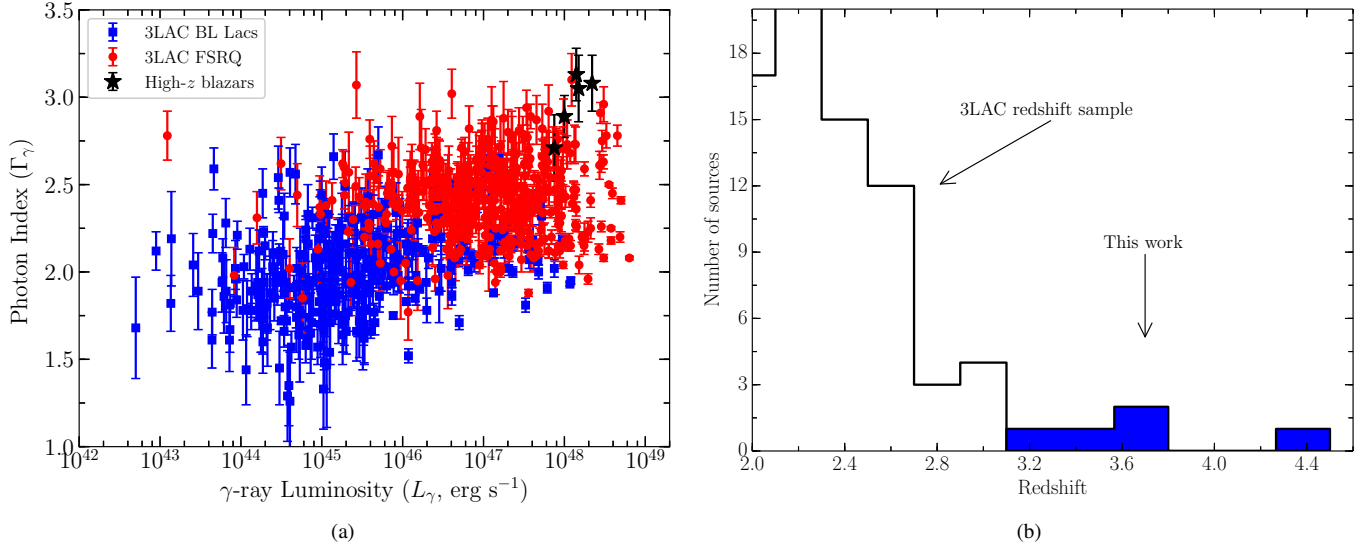


Figure 2. Comparison of new γ -ray detected high- z blazars with 3LAC objects in, left: γ -ray luminosity vs. photon index plane, and right: the redshift histogram. The plotted L_γ and Γ_γ are derived for the 0.1–300 GeV energy band, both for 3LAC and high- z blazars newly detected in γ -rays, for an equal comparison.

Mathur, S., & Elvis, M. 1995, *AJ*, 110, 1551
 Mattox, J. R., Bertsch, D. L., Chiang, J., et al. 1996, *ApJ*, 461, 396
 Tatischeff, V., Tavani, M., von Ballmoos, P., et al. 2016, arXiv:1608.03739
 Moran, E. C., & Helfand, D. J. 1997, *ApJL*, 484, L95
 Paliya, V. S., Parker, M. L., Fabian, A. C., & Stalin, C. S. 2016, *ApJ*, 825, 74
 Romani, R. W. 2006, *AJ*, 132, 1959
 Romani, R. W., Sowards-Emmerd, D., Greenhill, L. & Michelson, P., 2004, *ApJL*, 610, 9
 Sbarrato, T., Ghisellini, G., Tagliaferri, G., et al. 2015, *MNRAS*, 446, 2483
 Sbarrato, T., Tagliaferri, G., Ghisellini, G., et al. 2013, *ApJ*, 777, 147
 Schmidt, M. 1968, *ApJ*, 151, 393
 Shakura, N. I., & Sunyaev, R. A. 1973, *A&A*, 24, 337

Shen, Y., Richards, G. T., Strauss, M. A., et al. 2011, *ApJS*, 194, 45
 Sikora, M., Begelman, M. C., & Rees, M. J. 1994, *ApJ*, 421, 153
 Sikora, M., Błażejowski, M., Moderski, R., & Madejski, G. M. 2002, *ApJ*, 577, 78
 Torrealba, J., Chavushyan, V., Cruz-González, I., et al. 2012, *RMxAA*, 48, 9
 Vestergaard, M., & Peterson, B. M. 2006, *ApJ*, 641, 689
 Volonteri, M., Haardt, F., Ghisellini, G., & Della Ceca, R. 2011, *MNRAS*, 416, 216
 Wu, J., Brandt, W. N., Miller, B. P., et al. 2013, *ApJ*, 763, 109

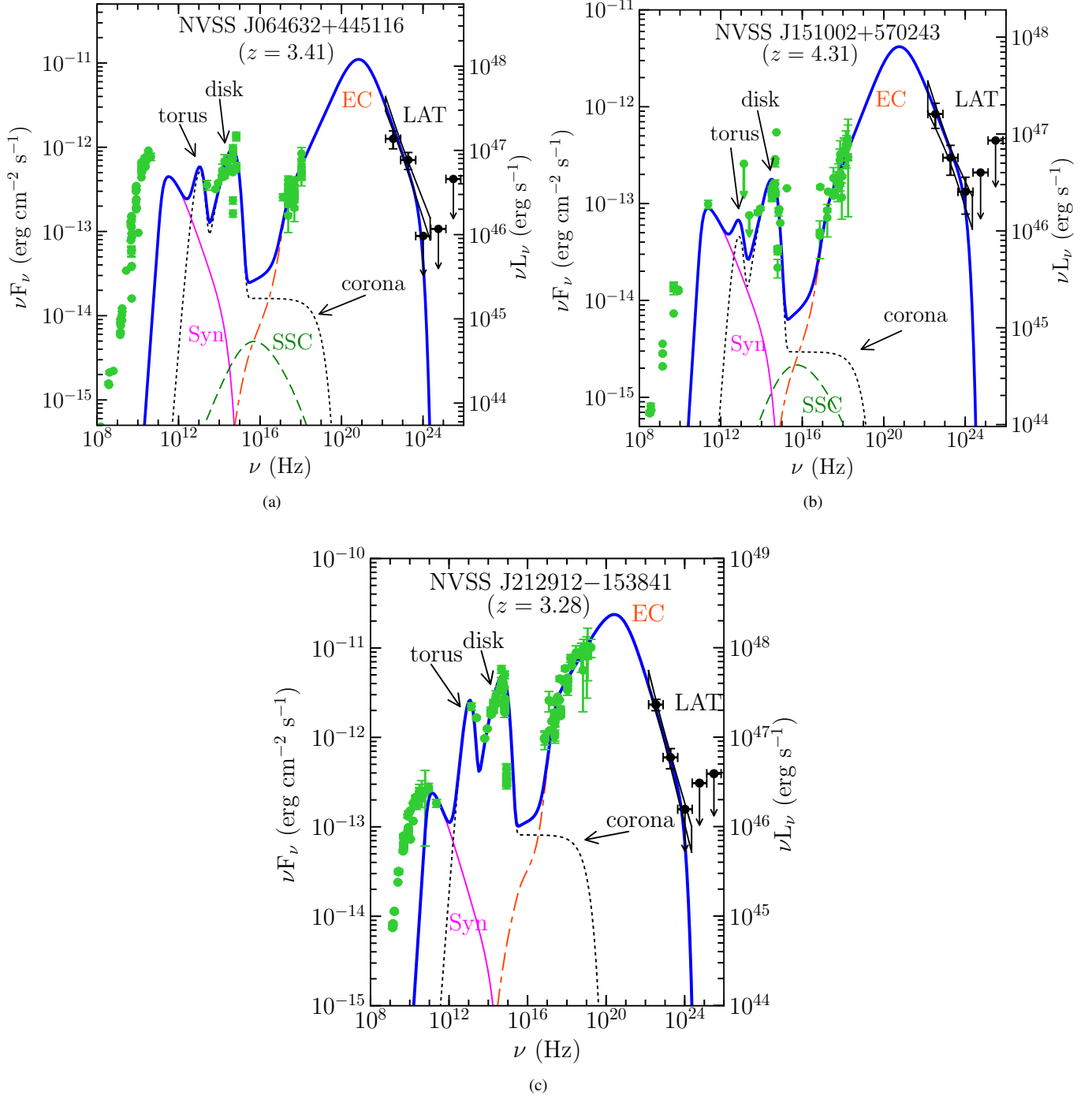


Figure 3. The broadband SEDs of three quasars reproduced using the one zone leptonic emission model. Lime green data points are the archival observations (<http://tools.asdc.asi.it/SED/>) and *Fermi*-LAT data points and bow-tie plots are in black. The dotted black line represents thermal radiations from the IR-torus, the accretion disk, and the X-ray corona, whereas, pink thin solid, green long dashed, and orange long-dash-dot lines correspond to non-thermal synchrotron, SSC, and EC emissions, respectively. The blue thick solid line denotes the sum of the contributions from all the radiative components.